

IGNOR: Image-guided Neural Object Rendering

Justus Thies¹ Michael Zollhöfer² Christian Theobalt³ Marc Stamminger⁴ Matthias Nießner¹

¹Technical University of Munich ²Stanford University

³Max-Planck-Institute for Informatics ⁴University of Erlangen-Nuremberg

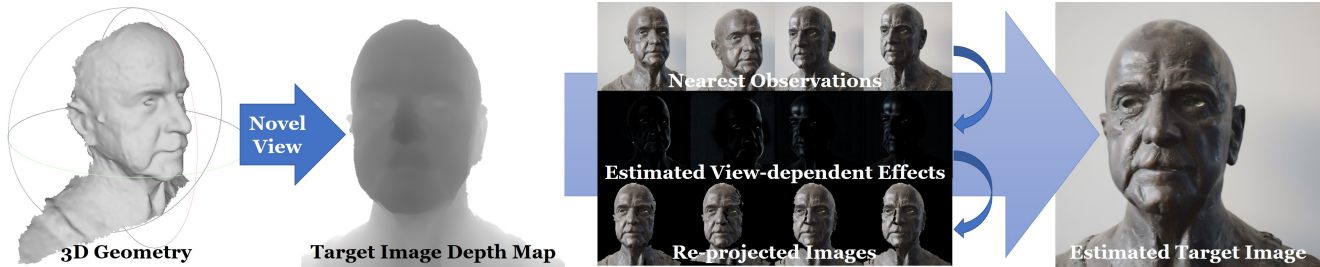


Figure 1: Input to our image-guided neural object rendering approach is a set of color images. We first reconstruct a geometric object proxy that is used to render a depth map of a novel view. In addition, we retrieve a set of nearest neighbor observations. Our network then synthesizes the corresponding color image by separating view-dependent and view-independent effects, warps the view-independent effects, while regressing the view-dependent effects of the target view. Finally, a composition network learns to combine all information.

Abstract

We propose a new learning-based novel view synthesis approach for scanned objects that is trained based on a set of multi-view images. Instead of using texture mapping or hand-designed image-based rendering, we directly train a deep neural network to synthesize a view-dependent image of an object. First, we employ a coverage-based nearest neighbour look-up to retrieve a set of reference frames that are explicitly warped to a given target view using cross-projection. Our network then learns to best composite the warped images. This enables us to generate photo-realistic results, while not having to allocate capacity on “remembering” object appearance. Instead, the multi-view images can be reused. While this works well for diffuse objects, cross-projection does not generalize to view-dependent effects. Therefore, we propose a decomposition network that extracts view-dependent effects and that is trained in a self-supervised manner. After decomposition, the diffuse shading is cross-projected, while the view-dependent layer of the target view is regressed. We show the effectiveness of our approach both qualitatively and quantitatively on real as well as synthetic data.

1. Introduction

In recent years, large progress has been made in 3D shape reconstruction of objects from photographs or depth streams. However, highly realistic re-rendering of such objects, e.g., in a virtual environment, is still very challenging. The reconstructed surface models and color information often exhibit inaccuracies or are comparably coarse [25, 39]. Many objects also exhibit strong view-dependent appearance effects, such as specularities. These effects not only frequently cause errors already during image-based shape reconstruction, but are also hard to reproduce when re-rendering an object from novel viewpoints. Static diffuse textures are frequently reconstructed for novel viewpoint synthesis, but these textures lack view-dependent appearance effects. Image-based rendering (IBR) introduced variants of view-dependent texturing that weightedly blend input images on the shape [6, 21, 7, 56]. This enables at least coarse approximation of view-dependent effects. However, these approaches often produce ghosting artifacts due to view blending on inaccurate geometry, or artifacts at occlusion boundaries. Some algorithms reduce these artifacts by combining view blending and optical flow correction [12, 8, 11], or by combining view-dependent blending with view-specific geometry [10, 20] or geometry with soft 3D visibility [41].

The idea of *IGNOR* is to leverage deep learning techniques to improve the re-rendering of objects that are reconstructed from a set of multi-view images. To this end, we first reconstruct a coarse geometric proxy of the object from multi-view images using a photogrammetric approach and cast re-rendering as a novel view synthesis problem. Similar to previous IBR techniques, we employ the reconstructed geometry as a proxy for reprojecting a subset of K nearby input images to the target view. The core innovation are two novel neural networks trained to combine the reprojected images in a target view:

First, a neural network called *EffectsNet* is trained in a self-supervised manner to estimate view-dependent effects, for example, specular highlights or reflections. The *EffectsNet* is used to remove view-dependent effects from the input images before reprojection and to re-insert these effects to the target views in a smooth and stable manner. Second, the *CompositionNet* composites the K re-projected images to a final output image. The *CompositionNet* is trained to be robust to reprojection errors and to fill regions where no image content is available. Both networks are trained per object, and can thus learn object-specific features of geometry, texture, and appearance. *IGNOR* clearly improves over previous novel view synthesis approaches in several ways: (1) it synthesizes highly realistic view-dependent appearance, (2) it learns to minimize ghosting and occlusion boundary artifacts that previously occurred with coarse proxy geometry, (3) it learns to fill holes that stem from occlusions, and it (4) synthesizes temporally smooth view interpolations with varying viewpoints without popping artifacts.

We demonstrate the effectiveness of our algorithm using synthetic and real data. Comparisons to texture-based and image-based rendering techniques, as well as to image-to-image translation methods are provided.

To summarize, the key contributions of our approach are:

- A novel neural network that predicts view-dependent effects, such as specular highlights, and can be used to compute diffuse renderings of an object,
- a self-supervised training approach for this network,
- an image-based rendering technique that enables novel view synthesis based on selected reference views that are converted to diffuse images,
- a composition network that optimally combines the reprojected reference frames to the final output.

2. Related Work

IGNOR is a method that intersects several research areas, each of which we review in a separate subsection.

Multi-view 3D Reconstruction Our approach builds on a coarse geometric proxy that is obtained using multi-view image-based 3D reconstruction. In the last decade, there has been a lot of progress in the field of image-based 3D reconstruction. Large-scale 3D models have been automatically obtained from images downloaded from the internet [2]. Camera poses and intrinsic calibration parameters are estimated based on structure-from-motion [27, 46], which can be implemented based on a global bundle adjustment step [51]. Afterwards, based on the camera poses and calibration, a dense three-dimensional pointcloud of the scene can be obtained using a multi-view stereo reconstruction approach [49, 17, 15]. Finally, a triangulated surface mesh is obtained, for example using Poisson surface reconstruction [29]. Even specular objects can be well reconstructed [16]. In this work, we obtain the mesh-based geometric proxy based on the COLMAP [47] 3D reconstruction approach.

Learning-based Image Synthesis Deep learning methods can improve quality in many realistic image synthesis tasks. Historically, many of these approaches have been based on generator networks following an encoder-decoder architecture [22, 33], such as a U-Net [44] with skip connections. Very recently, adversarially trained networks [18, 24, 38, 43] have shown some of the best result quality for various image synthesis tasks. For example, generative CNN models to synthesize body appearance [13], body articulation [9], body pose and appearance [59, 36], and face rendering [31] have been proposed. The DeepStereo [14] approach trains a neural network for view synthesis based on a large set of posed images. Tulsiani et al. [52] employ view synthesis as a proxy task to learn a layered scene representation. View synthesis can be learned directly from light field data [28]. Appearance Flow [58] learns an image warp based on a dense flow field to map information from the input to the target view. Zhou et al. [57] learn to extrapolate stereo views from imagery captured by a narrow-baseline stereo camera. Park et al. [40] explicitly decouple the view synthesis problem into an image warping and inpainting task. CNNs trained for image-to-image translation [23] could theoretically be applied to novel view synthesis, also with assistance of a shape proxy. However, we experimentally show that this leads to inferior results compared to our algorithm. Hedman et al. [19] use a CNN to learn a view blending function for image-based rendering with view-dependent shape proxies. In contrast, our approach learns to combine input views and to explicitly separate view-dependent effects which leads to superior reproduction of view-dependent appearance.

Image-based Rendering Our approach is related to image-based rendering (IBR) algorithms that cross-project input views to the target via a geometry proxy, and view-

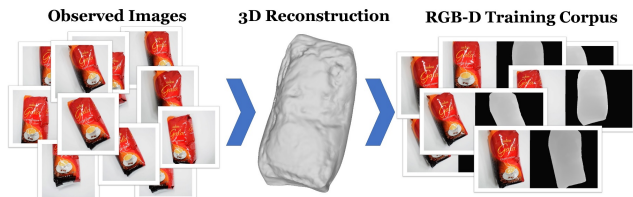


Figure 2: Input data preprocessing: based on a set of multi-view images we first reconstruct a coarse 3D model. The camera poses estimated during reconstruction and the 3D model are then used to render synthetic depth maps for the input views.

independently blend the re-projected views [6, 21, 7, 56]. Many previous IBR approaches exhibit ghosting artifacts due to view blending on inaccurate geometry, or exhibit artifacts at occlusion boundaries. Some methods try to reduce these artifacts by combining view blending and optical flow correction [12, 8, 11], by using view-specific geometry proxies [10, 20], or by encoding uncertainty in geometry as soft 3D visibility [41]. Our learning-based algorithm improves over the quality of these classical IBR approaches.

Intrinsic Decomposition Intrinsic decomposition tackles the ill-posed problem of splitting an image into a set of layers that correspond to physical quantities such as surface reflectance, diffuse shading, and/or specular shading. The decomposition of monocular video into reflectance and shading is classically approached based on a set of hand-crafted priors [4, 55, 55, 37]. Other approaches specifically tackle the problem of estimating [35] or removing specular highlights [54]. Highlight removal is of particular interest for images of faces [34]. A diffuse/specular separation can also be obtained based on a set of multi-view images captured under varying illumination [50]. The learning-based approach of Wu et al. [53] converts a set of multi-view images of a specular object into corresponding diffuse images. An extensive overview is given in the survey paper of Bonneel et al. [3]. To reuse the image content from the observed images to synthesize novel views, we are learning the decomposition into a diffuse and a view-dependent part in a self-supervised manner.

3. Overview

We propose a learning-based approach called *IGNOR* that enables novel view synthesis for arbitrary objects. Input to our approach is a set of N images $\mathcal{I} = \{\mathcal{I}_k\}_{k=1}^N$ of an object. In a preprocess, we obtain camera pose estimates and a coarse proxy geometry using the *COLMAP* [47, 48] structure-from-motion approach. We use the reconstruction and the camera poses to render synthetic depth maps \mathcal{D}_k for all input images \mathcal{I}_k to obtain the training corpus $\mathcal{T} = \{(\mathcal{I}_k, \mathcal{D}_k)\}_{k=1}^N$, see Fig. 2.

Based on this input, our learning-based approach gen-

erates novel views based on the stages that are depicted in Fig. 1. First, we employ a coverage-based look-up to select a small number $K \ll N$ of reference views from a subset of the training corpus. Given a depth map as input, our *EffectsNet* predicts the view-dependent effects for each reference view and thus the corresponding view-independent components can be obtained via subtraction (Sec. 4). The view-independent component is explicitly warped to the target view using geometry-guided cross-projection (Sec. 5). Next, the view-dependent effects for all warped reference views are predicted and added on top. Finally, our *CompositionNet* is used to optimally combine all warped reference views to generate the final output (Sec. 6). In the following, we discuss details, show how our approach can be trained (Sec. 7) based on our training corpus, and extensively evaluate our proposed approach (Sec. 8).

4. Decomposition (*EffectsNet*)

One of the main contributions of our work is a novel convolutional neural network that learns the disentanglement of view-dependent and view-independent illumination effects in a self-supervised manner. The network is based on a training corpus of multi-view images of the object, as shown in Fig. 3. Since our training data consists of a series of images taken from different viewing directions, assuming constant illumination, the reflected radiance of two corresponding points in two different images only differs by the view-dependent effects. Our self-supervised training procedure is based on a Siamese network [5] that gets a pair of randomly selected images from the training set as input. The task of the network is to extract view-dependent lighting effects from an image, based on geometric information from the proxy geometry.

Network Inputs Input to our network is a tensor that stacks a position, normal, view direction, and reflection direction map along the dimension of the channels. These inputs are inspired by the Phong illumination model [42]. We start with the depth map of the selected view and lift it to world space based on the camera intrinsic and extrinsic matrices. A per-pixel normal map in world space is then obtained via finite differences. Furthermore, we compute a vector field of per-pixel viewing directions that points from the surface towards the camera and a reflection direction map by mirroring the viewing direction along the per-pixel normal vector.

Network Architecture Our network Φ is an encoder-decoder network with skip connections, similar to U-Net [45]. The skip connections can directly propagate low-level features to the decoder. The encoder is based on 6 convolution layers (kernel size 4 and stride 2). The convolution

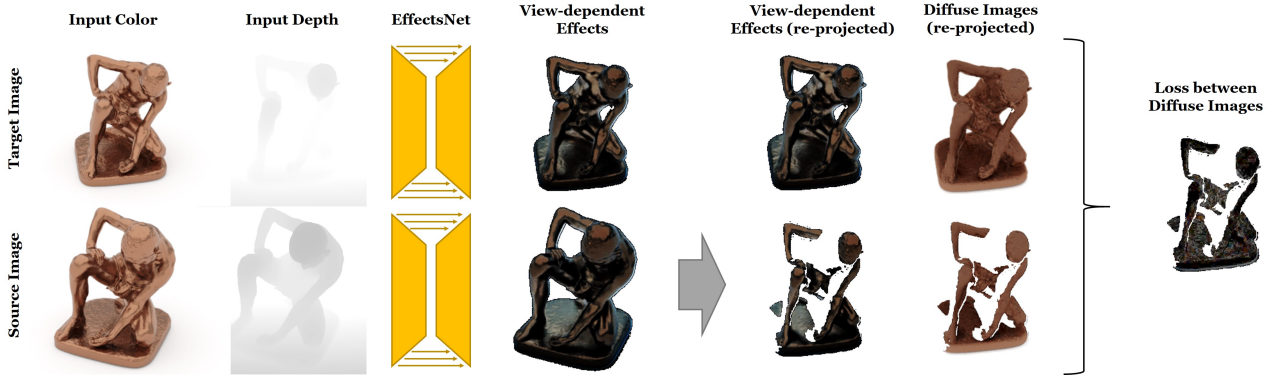


Figure 3: We propose a U-Net-like network called *EffectsNet*. The network is trained in a self-supervised fashion. Two random images from the training set are chosen in every optimization step and the network is used to predict the view-dependent effect of the images independently based on the respective depth map. After re-projecting the source image to the target image space we compute the diffuse color via subtraction. We optimize the network by minimizing the difference between the two diffuse images in the valid region.

layers output 32, 32, 64, 128, 256 and 512-dimensional feature maps, respectively. We use the ReLU activation function and normalize activations based on batchnorm. The decoder mirrors the encoder. We use transposed convolutions (kernel size 4 and stride 2) with the same number of feature channels as in the respective encoder layer. As final layer we use a 4×4 -convolution with a stride of 1 that outputs a 3-dimensional tensor that is fed to a Sigmoid to generate an image of the view-dependent illumination effects.

Self-supervised Training Since we assume constant illumination, the diffuse light reflected by a surface point is the same in every image, thus the appearance of a surface point only changes by the view-dependent components. We train our network in a self-supervised manner based on a Siamese network that predicts the view-dependent effects of two random views such that the difference of the diffuse aligned images (original image minus view-dependent effects) is minimal. To this end, we use the re-projection ability (see Sec. 5) to align pairs of input images, from which the view-dependent effects have been removed, and train the network to minimize the resulting differences in the overlap region of the two images. Given a randomly selected training pair $(\mathcal{I}_p, \mathcal{I}_q)$ and let $\Phi_{\Theta}(\mathbf{X}_t)$, $t \in \{p, q\}$ denote the output of the two Siamese towers. Then, our self-supervised loss for this training sample can be expressed as:

$$\mathcal{L}_q^p(\Theta) = \left\| M \circ \left[(\mathcal{I}_p - \Phi_{\Theta}(\mathbf{X}_p)) - \mathcal{W}_q^p (\mathcal{I}_q - \Phi_{\Theta}(\mathbf{X}_q)) \right] \right\|_2. \quad (1)$$

Here, \circ denotes the Hadamard product, Θ are the parameters of the encoder-decoder network Φ , which is shared between the two towers. M is a binary mask that is set to one if a surface point is visible in both views and zero otherwise. In addition we regularize the estimated view-dependent effects to be small w.r.t. an ℓ_1 -norm. This regularizer is weighted with 0.01 in our experiments. The cross-projection \mathcal{W}_q^p from image p to image q is based on the

geometric proxy (see Sec. 5). We train the network in a self-supervised fashion based on randomly selected pairs. The resulting network can then be used to compute the view-dependent effects of a novel view as well as to remove these from the reference images.

5. Stable Re-projection using *EffectsNet*

To generate a novel target view, we select a subset of K images based on a coverage-based nearest neighbor search. Each selected image is cross-projected to the target view, based on the proxy geometry. These images are finally used as input to our composition network *CompositionNet* (see Sec. 6) that fuses the information of the reference images into a single output image. In the following, we describe the coverage-based sampling and the cross-projection, and we show how to use our *EffectsNet* to achieve a robust re-projection of the view-dependent effects.

Coverage-based View Selection The selection of the $K \ll N$ used reference frames is based on surface coverage with respect to the target view. The goal is to have maximum coverage of the target view to ensure that texture information for the entire visible geometry is cross-projected. View selection is cast as an iterative process based on a greedy selection strategy that locally maximizes surface coverage. To this end, we start with 64×64 sample points on a uniform grid on the target view. In each iteration step, we search the view that has the largest overlap with the currently ‘uncovered’ region in the target view. We determine this view by cross-projecting the samples from the target view to the captured images, based on the reconstructed proxy geometry and camera parameters. A sample point in the target view is considered as covered, if it is also visible from the other view point, where visibility is determined based on an occlusion check. Each sample point that

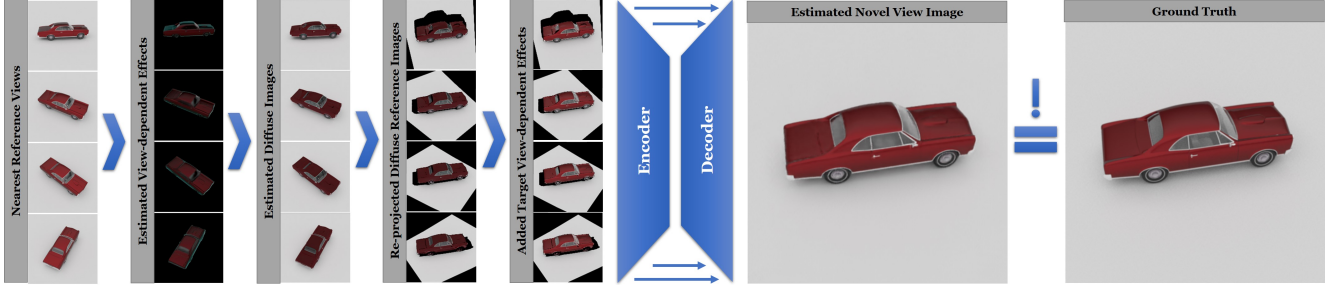


Figure 4: Overview of our compositing strategy: based on the nearest reference views, we predict the corresponding view-dependent effects using our *EffectsNet* architecture. The view-dependent effects are subtracted from the original images to get the diffuse images that can be re-projected into the target image space. In the target image space we estimate the final view-dependent effect and add them to the warped images. An encoder-decoder network is used to blend the reference images to obtain the final output image. During training, we enforce that the output image matches the corresponding ground truth image.

is covered by the finally selected view is invalidated for the next iteration steps. This procedure is repeated until the K best views have been selected.

To keep processing time low, we restrict this search to a small subset of the input images. This candidate set is taken from the training corpus and contains 20 images. We chose these candidates also based on a coverage-based selection scheme based on all frames of the training corpus. Note that this selection is done in a pre-processing step and is independent to the test phase.

Proxy-based Cross-projection We model the cross-projection \mathcal{W}_q^p from image p to image q based on the reconstructed geometric proxy and the camera parameters. Let $\mathbf{K}_p \in \mathbb{R}^{4 \times 3}$ denote the matrix of intrinsic parameters and $\mathbf{T}_p = [\mathbf{R}_p | \mathbf{t}_p] \in \mathbb{R}^{4 \times 4}$ the matrix of extrinsic parameters of view p . A similar notation holds for view q . Then, a homogeneous 2D screen space point $\mathbf{s}_p = (u, v, d)^T \in \mathbb{R}^3$ in view p , with depth being d , can be mapped to screen space of view q by:

$$\begin{aligned} \mathbf{s}_q &= \mathcal{W}_q^p(\mathbf{s}_p), \text{ with} \\ \mathcal{W}_q^p(\mathbf{s}_p) &= \mathbf{K}_q \mathbf{T}_q \mathbf{T}_p^{-1} \mathbf{K}_p^{-1} \mathbf{s}_p. \end{aligned} \quad (2)$$

We employ this mapping to cross-project color information from the reference views to a novel target view. To this end, we map every valid pixel (with a depth estimate) from the target view to the reference view. The color information from the reference view is sampled based on bilinear interpolation. Projected points that are occluded in the reference view or are not in the view frustum are invalidated. Occlusion is determined by a depth test w.r.t. the reference depth map. Applying the cross-projection to the set of all reference images, we get multiple warped references that match the novel target view point.

View-dependent Effects Image-based rendering methods often have problems with the re-projection of view-

dependent effects (see Sec. 8). In our image-guided pipeline, we solve this problem using our *EffectsNet* architecture. Before re-projection, we estimate the view-dependent effects from the input images using *EffectsNet* and subtract them. View-dependent effects are then re-inserted after re-projection, again using our *EffectsNet* architecture. By this, view-dependent effects are excluded from warping and generated in a stable manner.

6. Compositing (*CompositionNet*)

Finally, we composite the warped target views using another neural network called *CompositionNet*. Similar to the *EffectsNet*, our *CompositionNet* is an encoder-decoder network with skip connections. The network input is a tensor that stacks the K warped reference views, the corresponding warp fields as well as the target position map along the dimension of the channels and the output is a three channel RGB image. The encoder is based on 6 convolution layers (kernel size 4 and stride 2) with 64, 64, 128, 128, 256 and 256-dimensional feature maps, respectively. The activation functions are leaky ReLUs (negative slope of 0.2) in the encoder and ReLUs in the decoder. In both cases, we normalize all activations based on batchnorm. The decoder mirrors the encoder. We use transposed convolutions (kernel size 4 and stride 2) with the same number of feature channels as in the respective encoder layer. As final layer we use a 4×4 -convolution with a stride of 1 and a Sigmoid activation function that outputs the final image.

Loss function We are using an ℓ_1 -loss and an additional adversarial loss to measure the difference between the predicted output images and the ground truth data. The adversarial loss is based on the conditional PatchGAN loss that is also used in Pix2Pix [23]. In our experiments, we are weighting the adversarial loss with a factor of 0.01 and the ℓ_1 -loss with a factor of 1.0.

7. Network Training

In the following, we describe how we train the *EffectsNet* and *CompositionNet*. Both networks are trained independently using the Adam optimizer [32] built into Tensorflow [1]. Each network is trained for 64 epochs with a learning rate of 0.001 and the default parameters $\beta_1 = 0.9$, $\beta_2 = 0.999$, $\epsilon = 1 \cdot e^{-8}$. The networks are trained in an object-specific manner and from scratch each time.

7.1. Data Generation

Our training corpus $\mathcal{T} = \{(\mathcal{I}_k, \mathcal{D}_k)\}_{k=1}^N$ consists of N images \mathcal{I}_k and depth maps \mathcal{D}_k per object. In the following, we describe how we construct the training corpus for synthetic as well as real world data.



Figure 5: Renderings of our ground truth synthetic data. Based on the Mitsuba Renderer [26] we generate images of various objects that significantly differ in terms of material properties and shape.

Synthetic Training Data To generate photo-realistic synthetic imagery we employ the Mitsuba Renderer [26] to simulate global illumination effects. For each of the N views, we ray-trace a color image \mathcal{I}_k and its corresponding depth map \mathcal{D}_k . We extract a dense and smooth temporal camera path based on a spiral around the object. The camera is oriented at the center of the object. All images have a resolution of 512×512 and are rendered using path tracing with 96 samples per pixel and a maximum path length of 10. Fig. 5 illustrates various objects that we employ to test our approach. The objects differ significantly in terms of material properties and shape. Ranging from nearly diffuse materials (left) to the highly specular paint of the car (right). The size of the training sequence is 920, the test set contains 177 images.

Real World Training Data Our real world training data is captured using a *Nikon D5300* at a resolution of 1920×1080 pixels. Since we are relying on a sufficiently large set of images, we are recording videos of the objects at a frame rate of 30Hz. Based on *COLMAP* [47, 48] we reconstruct the camera path and a dense point cloud. We manually isolate the target object from other reconstructed geometry and run a Poisson reconstruction [30] step to extract the surface. We use this mesh to generate synthetic depth maps \mathcal{D}_k corresponding to the images \mathcal{I}_k (see Fig. 2). Finally, both, the

color and depth images are cropped and re-scaled to a resolution of 512×512 pixels. The training corpus ranges from 1000 to 1800 frames, depending on the sequence.

8. Results

In this section, we analyze our approach both qualitatively and quantitatively. We organized this section in two subsections that cover results on synthetic and real data. For all experiments we used $K = 4$ reference views per frame as shown in Fig. 4.

8.1. Experiments on Synthetic Data

Using synthetic data we are quantitatively analyzing the performance of our image-based texturing approach.

Evaluation of the *EffectsNet* In Fig. 6, we show a qualitative comparison of our predicted diffuse texture to the ground truth. The figure shows the results for a *Phong* rendering sequence. As can be seen, the estimated diffuse image is close to the ground truth.

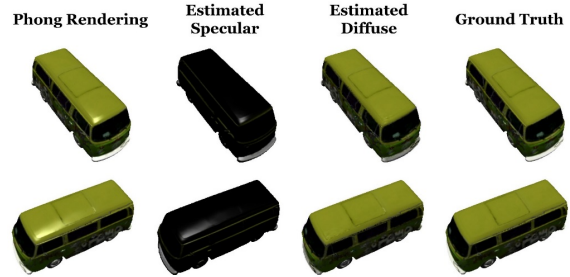


Figure 6: Comparison of the estimated diffuse images based on *EffectsNet* and the ground truth renderings. The input data has been synthesized by a standard *Phong* renderer written in *DirectX*. The training set contained 4900 images.

We also compared our technique with and without *EffectsNet* (see Fig. 7). The full pipeline results in smoother specular highlights and sharper details. On the test set the MSE without *EffectsNet* is 2.6876 versus 2.3864 with *EffectsNet*.

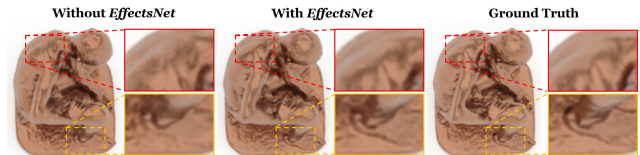


Figure 7: Image-guided rendering with and without *EffectsNet*. Without *EffectsNet* the specular highlights are not as smooth as the ground truth, also details get lost (see orange close-ups). Besides, the *EffectsNet* leads to a visually consistent temporal animation of the view-dependent effects.

Comparison to Pix2Pix To demonstrate the advantage of our new network architecture, we also compare to an image-to-image translation baseline (*Pix2Pix* [23]). *Pix2Pix* is trained to translate depth images into color images of the target object. As can be seen in Fig. 8, *Pix2Pix* does not generalize well to novel views. On our test set with 190 images, our method has a MSE of 1.12 while *Pix2Pix* results in a higher MSE of 36.63.

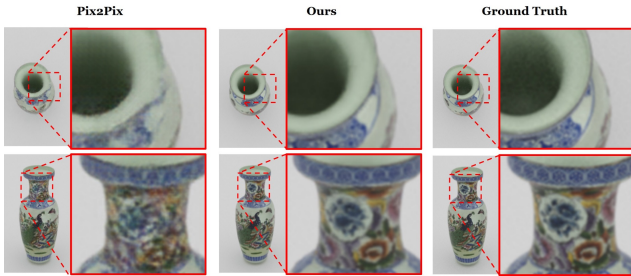


Figure 8: In comparison to *Pix2Pix*, we can see that our technique is able to generate images with correct detail as well as without blur artifacts. Both methods are trained on a dataset of 920 images.

Comparison to Image-based Rendering We compare our method to a baseline image-based rendering approach. The image-based rendering approach computes a per pixel average of the re-projected reference views. In contrast to our method, classical IBR techniques are not reproducing view-dependent effects as realistically and smoothly which can be seen in the top row of Fig. 9. IBR methods also suffer from occluded regions. Our method is able to in-paint these regions (shown in the bottom row of Fig. 9).

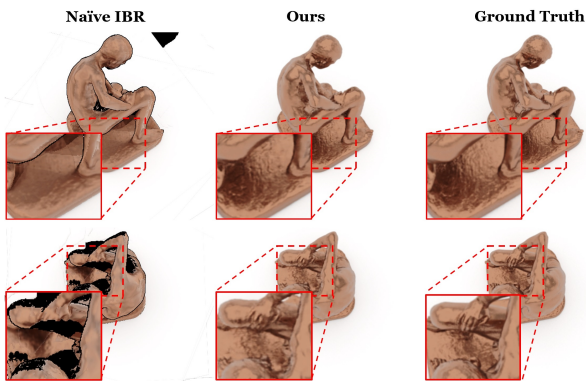


Figure 9: Comparison of a basic IBR baseline to our neural object rendering approach. The IBR method re-projects the colors from the reference views to the target image space. It fuses the images by computing a weighted pixel-wise average of the visible color values. It is not able to handle regions where no re-projected colors are available (black) and does not correctly handle view-dependent effects. The training set contained 1000 images.

Evaluation of Training Corpus Size In Fig. 10 we show the influence of the training corpus size on the quality of the results. While our method handles the reduction of the training data size well, the performance of *Pix2Pix* drastically decreases leading to a significantly higher MSE. When comparing these results to the results in Fig 8 it becomes evident that *Pix2Pix* has a significantly lower error on the bust sequence than on the vase sequence. The vase has much more details than the bust and, thus, is harder to reproduce.

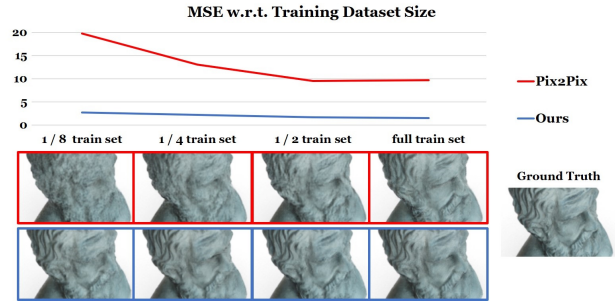


Figure 10: In this graph we compare the influence of the training corpus size on the MSE for our approach and *Pix2Pix*. The full dataset contains 920 images. We gradually half the size of the training set. As can be seen, the performance of our approaches degrades more gracefully than *Pix2Pix*.

8.2. Experiments on Real Data

In this section, we evaluate our algorithm on real data. Our focus lies on the visual quality of the re-rendering of objects including view-dependent effects. The advantages of our approach can best be seen in the supplemental video. We show re-rendered sequences of real objects such as shown in Fig. 11 - 15. In the following paragraphs, we detail the differences of our approach to existing methods.

Extracting View-dependent Effects Fig. 11 shows the effectiveness of our *EffectsNet* applied on a real sequence of an object. The globe has a specular surface and reflects the ceiling lights. These specular highlights are estimated and removed from the original image of the object which results in a diffuse image of the object.

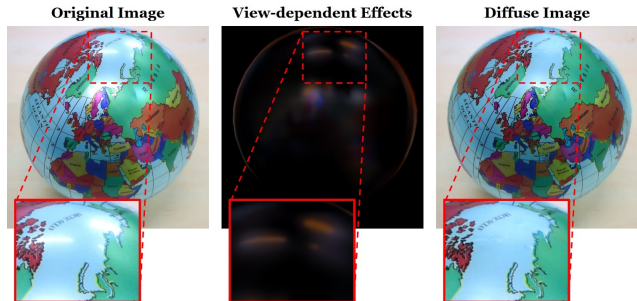


Figure 11: Prediction and removal of view-dependent effects of a real object with a highly specular surface.

Comparison to Texture-based Rendering Nowadays, most reconstruction frameworks like COLMAP [47], KinectFusion [25], or VoxelHashing [39] output a mesh with per-vertex colors or with a texture, which is the de facto standard in computer graphics. Fig. 12 shows a side-by-side comparison of our method and the rendering using per-vertex colors as well as using a static texture. Since both the vertex colors as well as the texture are static, these approaches are not able to capture the view dependent effects. Thus, view-dependent effects are backed into the vertex colors or texture and stay fixed (seen close-ups in Fig. 12).

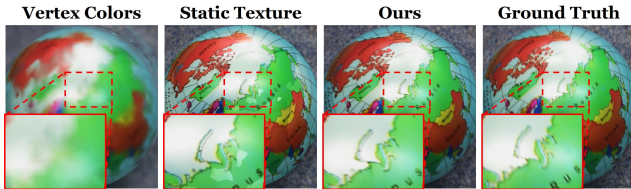


Figure 12: Image synthesis on real data in comparison to classical rendering approaches from computer graphics based on 20 reference views. From left to right: Poisson reconstructed mesh with per-vertex colors, texture-based rendering, our results and the ground truth. Every texel of the texture is a cosine-weighted sum of the data of four views where the normal points towards the camera the most.

Comparison to Image-based Rendering Fig. 13 shows a comparison of our method to image-based rendering. As can be seen the reconstruction of the object is imperfect, which leads to re-projection errors. Our method is able to handle such imperfections and inpaints regions with missing data.

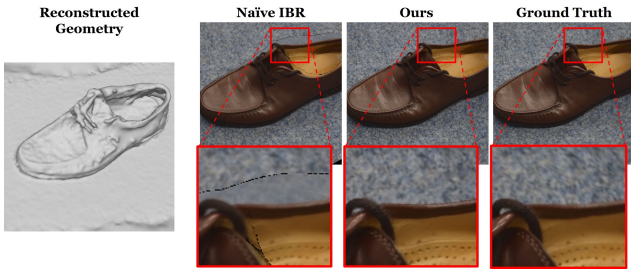


Figure 13: Image synthesis on real data: we show a comparison to a naïve IBR technique. From left to right: reconstructed geometry of the object, result of IBR, our result, and the ground truth.

Comparison to Learned Image Synthesis In Fig. 14 we show a comparison to *Pix2Pix*. Similar to the synthetic experiments, our method results in higher quality. In addition to the image-to-image translation network, we also implemented a method that is similar to Hedman et al. [19]. The idea is to use a neural network to predict blending weights

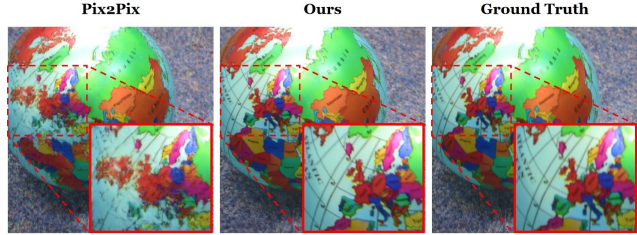


Figure 14: Comparison to *Pix2Pix* on real data. The close-up shows the artifacts that occur with *Pix2Pix* and are resolved by our approach leading to higher fidelity results.

for a image-based rendering composition. We are using a U-Net to predict the blending weights for a per-pixel convex combination of the reference views. The structure is the same as for our *CompositionNet*, except that the final layer is exchanged by a convolution that outputs a weight map for each reference view based on softmax. As input the network consumes the re-projected reference images as well as the warping fields and the position map of the target view. As can be seen in Fig. 15, the learned IBR method is not able to handle the changes of appearance that stem from view-dependent effects, there are still seams visible.

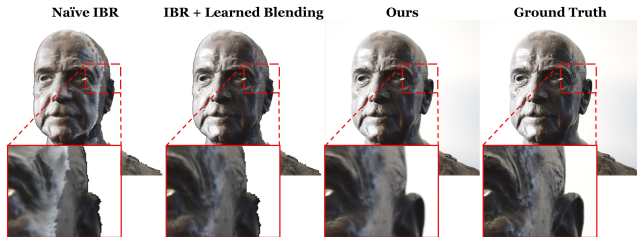


Figure 15: Comparison to a learned image-based rendering technique that predicts the blending weights for the re-projected reference views. Our approach achieves higher quality outputs.

9. Conclusion & Discussion

In this paper we proposed a novel image-guided rendering approach that outputs photo-realistic images of an object. We conducted several comparisons to state-of-the-art rendering techniques where we show similar or superior results. Still, our approach has a few limitations, which can be tackle in the future: The reconstruction stage is offline and takes about an hour for each object, a similar amount of time is spent to train each the *EffectsNet* and *CompositionNet*. At test time our approach runs at interactive rates, the inference time of the *EffectsNet* is 50Hz, while the *CompositionNet* runs with 10Hz on an Nvidia 1080Ti. Note, most of the network capacity of the *CompositionNet* is used to inpaint regions where data is missing (especially, the background). Similar to other learning based approaches, the method outputs results with heavy artifacts if the novel viewpoint is far from the training set.

The current network architecture does not leverage the ability of using temporal information, i.e., warping a previous generated image to the current frame. We think this is an interesting direction for future work. Nevertheless, our approach already works well on a variety of challenging scenes and shows promising results that are on-par or even surpass the current state-of-the-art methods. We hope it is a first step towards the goal of deep neural view synthesis for arbitrary objects and will inspire follow-up work.

Acknowledgements

We thank Angela Dai for the video voice over. This work is funded by a Google Research Grant, supported by the ERC Starting Grant Scan2CAD (804724), ERC Starting Grant CapReal (335545), and the ERC Consolidator Grant 4DRepLy (770784), the Max Planck Center for Visual Computing and Communication (MPC-VCC), a TUM-IAS Rudolf Mößbauer Fellowship (Focus Group Visual Computing), and a Google Faculty Award.

References

- [1] M. Abadi, A. Agarwal, P. Barham, E. Brevdo, Z. Chen, C. Citro, G. S. Corrado, A. Davis, J. Dean, M. Devin, S. Ghemawat, I. Goodfellow, A. Harp, G. Irving, M. Isard, Y. Jia, R. Jozefowicz, L. Kaiser, M. Kudlur, J. Levenberg, D. Mané, R. Monga, S. Moore, D. Murray, C. Olah, M. Schuster, J. Shlens, B. Steiner, I. Sutskever, K. Talwar, P. Tucker, V. Vanhoucke, V. Vasudevan, F. Viégas, O. Vinyals, P. Warden, M. Wattenberg, M. Wicke, Y. Yu, and X. Zheng. TensorFlow: Large-scale machine learning on heterogeneous systems, 2015. Software available from tensorflow.org. 6
- [2] S. Agarwal, Y. Furukawa, N. Snavely, I. Simon, B. Curless, S. M. Seitz, and R. Szeliski. Building rome in a day. *Commun. ACM*, 54(10):105–112, Oct. 2011. 2
- [3] N. Bonneel, B. Kovacs, S. Paris, and K. Bala. Intrinsic Decompositions for Image Editing. *Computer Graphics Forum (Eurographics State of the Art Reports 2017)*, 36(2), 2017. 3
- [4] N. Bonneel, K. Sunkavalli, J. Tompkin, D. Sun, S. Paris, and H. Pfister. Interactive Intrinsic Video Editing. *ACM Transactions on Graphics (SIGGRAPH Asia 2014)*, 33(6), 2014. 3
- [5] J. Bromley, I. Guyon, Y. LeCun, E. Säckinger, and R. Shah. Signature verification using a “siamese” time delay neural network. In *Proceedings of the 6th International Conference on Neural Information Processing Systems, NIPS’93*, pages 737–744, San Francisco, CA, USA, 1993. Morgan Kaufmann Publishers Inc. 3
- [6] C. Buehler, M. Bosse, L. McMillan, S. Gortler, and M. Cohen. Unstructured lumigraph rendering. In *Proceedings of the 28th Annual Conference on Computer Graphics and Interactive Techniques, SIGGRAPH ’01*, pages 425–432, New York, NY, USA, 2001. ACM. 1, 3
- [7] J. Carranza, C. Theobalt, M. A. Magnor, and H.-P. Seidel. Free-viewpoint video of human actors. *ACM Trans. Graph. (Proc. SIGGRAPH)*, 22(3):569–577, July 2003. 1, 3
- [8] D. Casas, C. Richardt, J. P. Collomosse, C. Theobalt, and A. Hilton. 4d model flow: Precomputed appearance alignment for real-time 4d video interpolation. *Comput. Graph. Forum*, 34(7):173–182, 2015. 1, 3
- [9] C. Chan, S. Ginosar, T. Zhou, and A. A. Efros. Everybody Dance Now. *ArXiv e-prints*, Aug. 2018. 2
- [10] G. Chaurasia, S. Duchene, O. Sorkine-Hornung, and G. Drettakis. Depth synthesis and local warps for plausible image-based navigation. *ACM Trans. Graph.*, 32(3):30:1–30:12, July 2013. 1, 3
- [11] R. Du, M. Chuang, W. Chang, H. Hoppe, and A. Varshney. Montage4d: Interactive seamless fusion of multiview video textures. In *Proceedings of the ACM SIGGRAPH Symposium on Interactive 3D Graphics and Games, I3D ’18*, pages 5:1–5:11, New York, NY, USA, 2018. ACM. 1, 3
- [12] M. Eisemann, B. De Decker, M. Magnor, P. Bekaert, E. De Aguiar, N. Ahmed, C. Theobalt, and A. Sellent. Floating Textures. *Computer Graphics Forum (Proc. EUROGRAPHICS)*, 2008. 1, 3
- [13] P. Esser, E. Sutter, and B. Ommer. A variational u-net for conditional appearance and shape generation. *CoRR*, abs/1804.04694, 2018. 2
- [14] J. Flynn, I. Neulander, J. Philbin, and N. Snavely. Deepstereo: Learning to predict new views from the world’s imagery. In *The IEEE Conference on Computer Vision and Pattern Recognition (CVPR)*, 2016. 2
- [15] A. Geiger, J. Ziegler, and C. Stiller. Stereoscan: Dense 3d reconstruction in real-time. In *Intelligent Vehicles Symposium*, pages 963–968. IEEE, 2011. 2
- [16] C. Godard, P. Hedman, W. Li, and G. J. Brostow. Multi-view Reconstruction of Highly Specular Surfaces in Uncontrolled Environments. In *3DV*, 2015. 2
- [17] M. Goesele, N. Snavely, B. Curless, H. Hoppe, and S. M. Seitz. Multi-view stereo for community photo collections. In *ICCV*, pages 1–8. IEEE Computer Society, 2007. 2
- [18] I. J. Goodfellow, J. Pouget-Abadie, M. Mirza, B. Xu, D. Warde-Farley, S. Ozair, A. Courville, and Y. Bengio. Generative adversarial nets. 2014. 2
- [19] P. Hedman, J. Philip, T. Price, J.-M. Frahm, G. Drettakis, and G. Brostow. Deep blending for free-viewpoint image-based rendering. *ACM Transactions on Graphics (SIGGRAPH Asia Conference Proceedings)*, 37(6), November 2018. 2, 8
- [20] P. Hedman, T. Ritschel, G. Drettakis, and G. Brostow. Scalable Inside-Out Image-Based Rendering. 35(6):231:1–231:11, 2016. 1, 3
- [21] B. Heigl, R. Koch, M. Pollefeys, J. Denzler, and L. J. V. Gool. Plenoptic modeling and rendering from image sequences taken by hand-held camera. In *Proc. DAGM*, pages 94–101, 1999. 1, 3
- [22] G. E. Hinton and R. Salakhutdinov. Reducing the dimensionality of data with neural networks. *Science*, 313(5786):504–507, July 2006. 2
- [23] P. Isola, J.-Y. Zhu, T. Zhou, and A. A. Efros. Image-to-image translation with conditional adversarial networks. *arxiv*, 2016. 2, 5, 7
- [24] P. Isola, J.-Y. Zhu, T. Zhou, and A. A. Efros. Image-to-image translation with conditional adversarial networks. pages 5967–5976, 2017. 2
- [25] S. Izadi, D. Kim, O. Hilliges, D. Molyneaux, R. Newcombe, P. Kohli, J. Shotton, S. Hodges, D. Freeman, A. Davison, and A. Fitzgibbon. Kinectfusion: Real-time 3d reconstruction and interaction using a moving depth camera. In *Proceedings of the 24th Annual ACM Symposium on User Interface Software and Technology, UIST ’11*, pages 559–568, New York, NY, USA, 2011. ACM. 1, 8
- [26] W. Jakob. Mitsuba renderer, 2010. <http://www.mitsuba-renderer.org>. 6
- [27] T. Jebara, A. Azarbayejani, and A. Pentland. 3d structure from 2d motion. *IEEE Signal Processing Magazine*, 16(3):66–84, May 1999. 2
- [28] N. K. Kalantari, T.-C. Wang, and R. Ramamoorthi. Learning-based view synthesis for light field cameras. *ACM Transactions on Graphics (Proceedings of SIGGRAPH Asia 2016)*, 35(6), 2016. 2
- [29] M. Kazhdan, M. Bolitho, and H. Hoppe. Poisson surface reconstruction. In *Proceedings of the Fourth Eurographics Symposium on Geometry Processing, SGP ’06*, pages 61–70, Aire-la-Ville, Switzerland, Switzerland, 2006. Eurographics Association. 2
- [30] M. Kazhdan and H. Hoppe. Screened poisson surface reconstruction. *ACM Trans. Graph.*, 32(3):29:1–29:13, July 2013. 6
- [31] H. Kim, P. Garrido, A. Tewari, W. Xu, J. Thies, N. Nießner, P. Pérez, C. Richardt, M. Zollhöfer, and C. Theobalt. Deep Video Portraits. *ACM Transactions on Graphics 2018 (TOG)*, 2018. 2

- [32] D. P. Kingma and J. Ba. Adam: A method for stochastic optimization. *CoRR*, abs/1412.6980, 2014. [6](#)
- [33] D. P. Kingma and M. Welling. Auto-encoding variational bayes. *CoRR*, abs/1312.6114, 2013. [2](#)
- [34] C. Li, S. Lin, K. Zhou, and K. Ikeuchi. Specular highlight removal in facial images. In *2017 IEEE Conference on Computer Vision and Pattern Recognition (CVPR)*, pages 2780–2789, July 2017. [3](#)
- [35] S. Lin, Y. Li, S. B. Kang, X. Tong, and H.-Y. Shum. Diffuse-specular separation and depth recovery from image sequences. In *Proceedings of the 7th European Conference on Computer Vision-Part III, ECCV '02*, pages 210–224, Berlin, Heidelberg, 2002. Springer-Verlag. [3](#)
- [36] L. Liu, W. Xu, M. Zollhoefer, H. Kim, F. Bernard, M. Habermann, W. Wang, and C. Theobalt. Neural animation and reenactment of human actor videos, 2018. [2](#)
- [37] A. Meka, M. Zollhoefer, C. Richardt, and C. Theobalt. Live intrinsic video. *ACM Transactions on Graphics (Proceedings SIGGRAPH)*, 35(4), 2016. [3](#)
- [38] M. Mirza and S. Osindero. Conditional generative adversarial nets. arXiv:1411.1784, 2014. [2](#)
- [39] M. Nießner, M. Zollhöfer, S. Izadi, and M. Stamminger. Real-time 3d reconstruction at scale using voxel hashing. *ACM Transactions on Graphics (TOG)*, 2013. [1](#), [8](#)
- [40] E. Park, J. Yang, E. Yumer, D. Ceylan, and A. C. Berg. Transformation-grounded image generation network for novel 3d view synthesis. *CoRR*, abs/1703.02921, 2017. [2](#)
- [41] E. Penner and L. Zhang. Soft 3d reconstruction for view synthesis. *ACM Trans. Graph.*, 36(6):235:1–235:11, Nov. 2017. [1](#), [3](#)
- [42] B. T. Phong. Illumination for computer generated pictures. *Commun. ACM*, 18(6):311–317, June 1975. [3](#)
- [43] A. Radford, L. Metz, and S. Chintala. Unsupervised representation learning with deep convolutional generative adversarial networks. 2016. [2](#)
- [44] O. Ronneberger, P. Fischer, and T. Brox. U-Net: Convolutional networks for biomedical image segmentation. In *International Conference on Medical Image Computing and Computer-Assisted Intervention (MICCAI)*, pages 234–241, 2015. [2](#)
- [45] O. Ronneberger, P. Fischer, and T. Brox. U-net: Convolutional networks for biomedical image segmentation. In N. Navab, J. Hornegger, W. M. Wells, and A. F. Frangi, editors, *Medical Image Computing and Computer-Assisted Intervention – MICCAI 2015*, pages 234–241, Cham, 2015. Springer International Publishing. [3](#)
- [46] J. L. Schnberger and J. Frahm. Structure-from-motion revisited. In *2016 IEEE Conference on Computer Vision and Pattern Recognition (CVPR)*, pages 4104–4113, June 2016. [2](#)
- [47] J. L. Schönberger and J.-M. Frahm. Structure-from-Motion Revisited. In *Conference on Computer Vision and Pattern Recognition (CVPR)*, 2016. [2](#), [3](#), [6](#), [8](#)
- [48] J. L. Schönberger, E. Zheng, M. Pollefeys, and J.-M. Frahm. Pixel-wise View Selection for Unstructured Multi-View Stereo. In *European Conference on Computer Vision (ECCV)*, 2016. [3](#), [6](#)
- [49] S. M. Seitz, B. Curless, J. Diebel, D. Scharstein, and R. Szeliski. A comparison and evaluation of multi-view stereo reconstruction algorithms. In *Proceedings of the 2006 IEEE Computer Society Conference on Computer Vision and Pattern Recognition - Volume 1, CVPR '06*, pages 519–528, Washington, DC, USA, 2006. IEEE Computer Society. [2](#)
- [50] K. Takechi and T. Okabe. Diffuse-specular separation of multi-view images under varying illumination. In *2017 IEEE International Conference on Image Processing (ICIP)*, pages 2632–2636, Sept 2017. [3](#)
- [51] B. Triggs, P. F. McLauchlan, R. I. Hartley, and A. W. Fitzgibbon. Bundle adjustment - a modern synthesis. In *Proceedings of the International Workshop on Vision Algorithms: Theory and Practice, ICCV '99*, pages 298–372, London, UK, UK, 2000. Springer-Verlag. [2](#)
- [52] S. Tulsiani, R. Tucker, and N. Snavely. Layer-structured 3d scene inference via view synthesis. In *ECCV*, 2018. [2](#)
- [53] S. Wu, H. Huang, T. Portenier, M. Sela, D. Cohen-Or, R. Kimmel, and M. Zwicker. Specular-to-diffuse translation for multi-view reconstruction. In V. Ferrari, M. Hebert, C. Sminchisescu, and Y. Weiss, editors, *Computer Vision - ECCV 2018 - 15th European Conference, Munich, Germany, September 8-14, 2018, Proceedings, Part IV*, volume 11208 of *Lecture Notes in Computer Science*, pages 193–211. Springer, 2018. [3](#)
- [54] Q. Yang, J. Tang, and N. Ahuja. Efficient and robust specular highlight removal. *IEEE Trans. Pattern Anal. Mach. Intell.*, 37(6):1304–1311, 2015. [3](#)
- [55] G. Ye, E. Garces, Y. Liu, Q. Dai, and D. Gutierrez. Intrinsic video and applications. *ACM Trans. Graph.*, 33(4):80:1–80:11, July 2014. [3](#)
- [56] K. C. Zheng, A. Colburn, A. Agarwala, M. Agrawala, D. Salesin, B. Curless, and M. F. Cohen. Parallax photography: creating 3d cinematic effects from stills. In *Proc. Graphics Interface*, pages 111–118. ACM Press, 2009. [1](#), [3](#)
- [57] T. Zhou, R. Tucker, J. Flynn, G. Fyffe, and N. Snavely. Stereo magnification: Learning view synthesis using multiplane images. *ACM Trans. Graph.*, 37(4):65:1–65:12, July 2018. [2](#)
- [58] T. Zhou, S. Tulsiani, W. Sun, J. Malik, and A. A. Efros. View synthesis by appearance flow. In *ECCV*. 2016. [2](#)
- [59] H. Zhu, H. Su, P. Wang, X. Cao, and R. Yang. View extrapolation of human body from a single image. *CoRR*, abs/1804.04213, 2018. [2](#)